RESEARCH ARTICLE

Formalism of a Treatment-Modulated Logistic Map for Breast Tumor Growth: Mathematical Formulation, Nonlinear Dynamics, and Clinically Inspired Simulation

Matheus dos Santos Farias[1,*]

[1] Institute for Energy and Nuclear Research (IPEN), University of São Paulo, São Paulo 05508-220, Brazil

Abstract

This study develops a treatment-modulated discrete framework for breast-tumor dynamics, emphasizing dimensional consistency, treatment dependence, and the distinction between scalar tumor burden and spatial tumor-density fields. Starting from the dimensional logistic growth law, treatment is introduced through a cycle-dependent survival factor. Normalization by the continuous carrying capacity K_c yields the exact Euler update $y_{n+1} = S_n[y_n + g\Delta t_n y_n(1 - y_n)]$, whereas the canonical non-autonomous map $x_{n+1} = r_n x_n(1 - x_n)$, with $r_n = (1 + g\Delta t_n)S_n$, is retained as a reduced nonlinear benchmark. This distinction prevents discretization-induced period-doubling and chaos from being interpreted as intrinsic tumor behavior. Invariance and cumulative extinction conditions are derived for non-autonomous sequences $\{r_n\}$, including the periodic product criterion. Radiotherapy is coupled through the linear-quadratic survival model and chemotherapy through an $E_{\max}$ exposure-response formulation. A published breast-cancer case provides the clinical treatment chronology, including chemotherapy and 26 Gy radiotherapy delivered in five fractions. Because longitudinal tumor measurements, voxel-level dose maps, pharmacokinetic data, and tumor-specific radiosensitivity parameters are unavailable, no patient-specific calibration or dose-response validation is claimed. Geant4 outputs are therefore used as clinically inspired spatial visualizations, with dose-to-survival coupling explicitly formulated. The framework also incorporates primitive-parameter uncertainty propagation and state-sensitivity analysis, providing a consistent basis for future patient-specific modeling.

Keywords: logistic map, breast cancer, mathematical oncology, chemotherapy, radiotherapy, Geant4, nonlinear dynamics, Lyapunov exponent, bifurcation, treatment response.

1 Introduction

Breast cancer remains one of the leading causes of cancer-related mortality worldwide, with incidence and mortality patterns documented across diverse populations and health systems [1, 2]. The clinical complexity of advanced breast cancer—including large fungating masses, metastatic disease, and

Submitted: 27 July 2026
Revised: 05 September 2026
Accepted: 17 September 2026
Published: 20 September 2026

Vol. 2, **No.** 3, 2026.
10.62762/JNDA.2026.825872

***Corresponding author:**
✉ Matheus dos Santos Farias
matheusfariasfm@gmail.com

Citation
dos Santos Farias, M. (2026). Formalism of a Treatment-Modulated Logistic Map for Breast Tumor Growth: Mathematical Formulation, Nonlinear Dynamics, and Clinically Inspired Simulation. *Journal of Nonlinear Dynamics and Applications*, 2(3), 177–191.

multimodal treatment sequencing—motivates the development of mathematical frameworks that can describe tumor dynamics and treatment response in a dimensionally consistent and mechanistically interpretable way. Logistic models are widely used because they represent constrained growth through an intrinsic proliferation term and a carrying-capacity limitation. In breast cancer, logistic growth has also been parameterized from quantitative MRI measurements to estimate proliferation rates and predict cellularity during neoadjuvant chemotherapy, demonstrating that clinically acquired imaging can be used to populate mathematical tumor-growth models [3].

The continuous logistic growth law is classical [4], and the fixed points, stability thresholds, period-doubling cascade, and chaotic regimes of the discrete map obtained from it are well established [5]. Because these dynamical properties are already known, the contribution of the present work is neither the derivation of a new logistic map nor the introduction of new computational tools. A further limitation is essential for interpretation: the canonical map used here is obtained by forward-Euler discretization of a continuous logistic equation. Consequently, periodic and chaotic regimes at large values of the dimensionless step $g\Delta t$ describe the discrete recurrence and may reflect discretization-induced behavior rather than an intrinsic biological property of the continuous tumor-growth law. The nonlinear calculations are therefore interpreted as mathematical properties of the discrete model, not as evidence that an individual tumor is biologically chaotic.

This distinction between discretization-induced dynamics and intrinsic biological behavior is consistent with contemporary mathematical oncology, in which the reliability of quantitative predictions depends on whether model parameters are identifiable from the available time-course measurements [6]. For radiotherapy, treatment effects have been incorporated into logistic-type tumor models through linear-quadratic cell-survival formulations [7] and, alternatively, through treatment-induced dynamic modulation of the carrying capacity, as demonstrated in head-and-neck cancer [8]. These studies motivate the treatment coupling adopted here while also making clear that patient-specific calibration requires longitudinal measurements.

The clinical scenario used as a computational reference is the case reported by Hong et al. [9]. The patient presented with an approximately 10×12 cm fungating left-breast mass and metastatic disease. The reported treatment sequence comprised three cycles of weekly paclitaxel, three cycles of weekly doxorubicin, 26 Gy delivered in five consecutive daily radiotherapy fractions, and subsequent doxorubicin. The mass was reported as 0.8×1.8 cm on CT 3.5 months after radiotherapy. The published chronology therefore provides a clinically grounded sequence, but it does not provide the longitudinal measurements required to estimate every parameter of the proposed treatment-modulated recurrence [9].

The revised formulation consequently makes three distinctions throughout the manuscript: (i) the continuous logistic carrying capacity and the scaling introduced by Euler discretization are not identified as the same quantity; (ii) the treatment-dependent coefficient is defined only after a consistent dimensional update is specified, and the reduced canonical r_n representation is explicitly distinguished from the exact K_c-normalized update; and (iii) canonical logistic-map values are used only to study nonlinear regimes unless they have been calibrated to measurable clinical data.

2 Aim and Scope

The aim is to establish a mathematically consistent discrete framework in which tumor growth and treatment response can be connected without attributing clinical meaning to parameters that have not been estimated. The study therefore combines analytical derivation, treatment-dependent parameterization, numerical nonlinear-dynamics analysis, and clinically inspired three-dimensional visualization.

- Derive the discrete logistic recurrence and distinguish the continuous carrying capacity from the Euler scaling parameter.
- Define a dimensionless treatment-dependent coefficient r_n and identify the units and biological meaning of its constituent quantities.
- Specify how chemotherapy exposure and radiotherapy dose can enter the model through treatment-survival factors.
- Characterize the admissible state space and the classical fixed-point stability conditions.
- Provide a reproducible bifurcation analysis and Lyapunov-exponent calculation with explicit initial

Table 1. Components of the revised modeling workflow.

Component	Role	Output
Continuous logistic model	Represent untreated constrained tumor growth	g and K_c definitions
Treatment parameterization	Connect measurable treatment quantities to r_n	dimensionless r_n
Nonlinear-dynamics analysis	Characterize fixed points, bifurcation, and chaos	bifurcation and Lyapunov diagrams
Geant4/C++ visualization	Illustrate three-dimensional treatment chronology	normalized tumor-density fields
Clinical case report	Provide treatment sequence and reported endpoints	independent clinical reference

conditions, transient length, retained iterations, and numerical procedure.

- Separate the mathematical regime analysis from the clinically inspired Geant4 visualization and state the current limits of patient-specific validation.

3 Methodology

The revised workflow consists of four stages. First, a dimensional logistic growth model is written for tumor volume. Second, treatment is applied to the dimensional state, with the treatment operation explicitly ordered after the growth update in the formulation used here. Third, normalization by the continuous carrying capacity K_c produces a consistent non-autonomous recurrence; the canonical r_n logistic map is then analyzed separately as a reduced benchmark. Fourth, the published breast-cancer case is used as a clinical chronology for the three-dimensional Geant4 visualization. No clinical parameter is inferred when the source case does not report the information needed for that inference. Table 1 summarizes the four stages.

For the fixed-r dynamical analysis, the recurrence was iterated in double precision with $x_0 = 0.20$. The bifurcation calculation used 2,001 uniformly spaced values of r from 0 to 4, with $\Delta r = 0.002$; 1,000 iterations were discarded as a transient and the subsequent 300 iterations were retained for plotting. The Lyapunov exponent was estimated from 10,000 iterations after discarding the first 1,000. For the non-autonomous analysis, the same recurrence was evaluated with explicitly prescribed sequences $\{r_n\}$; the illustrative sequences reported below are mathematical examples and are not patient-specific treatment estimates.

4 Mathematical Formulation

4.1 Continuous logistic growth and the meaning of K_c

Let $T(t)$ denote tumor volume. The continuous logistic equation is

$$\frac{dT}{dt} = aT\left(1 - \frac{T}{K_c}\right), \tag{1}$$

where a is the intrinsic net proliferation rate with units of time^{-1} and K_c is the continuous carrying capacity with units of volume. Equivalently, the dimensional polynomial form is

$$\frac{dT}{dt} = aT - bT^2, \qquad K_c = \frac{a}{b}. \tag{2}$$

Here b has units of (volume·time)$^{-1}$. Thus $K_c = a/b$ is the equilibrium tumor volume of the continuous model. It should not be confused with the scale that appears when a forward-Euler discretization is transformed into the canonical logistic map.

Using $t_n = n\Delta t$ and the forward-Euler approximation gives

$$T_{n+1} = T_n + \Delta t\left(aT_n - bT_n^2\right). \tag{3}$$

Factoring the right-hand side defines the Euler scaling quantity

$$K_E = \frac{1 + a\Delta t}{b\Delta t} \tag{4}$$

and therefore

$$T_{n+1} = (1 + a\Delta t)T_n\left(1 - \frac{T_n}{K_E}\right). \tag{5}$$

The quantity K_E has units of volume, but it is a discretization scale, not the continuous equilibrium K_c. In fact, K_E is not equal to K_c for finite Δt; since $K_E = K_c + 1/(b\Delta t)$, it diverges as $\Delta t \to 0$ rather than approaching K_c. When Δt is allowed to vary with treatment cycle, the corresponding Euler scale $K_{E,n} = (1 + g\Delta t_n)/(b\Delta t_n)$ also varies. Thus, using $x_n = T_n/K_{E,n}$ as the state variable would introduce an additional factor $K_{E,n}/K_{E,n+1}$ into the recurrence. The canonical form $x_{n+1} = r_n x_n(1 - x_n)$ cannot

therefore be obtained by simply replacing Δt with Δt_n while keeping a time-independent normalization. This is the normalization issue addressed explicitly in Sec. 4.3.

Defining $x_n = T_n/K_E$ yields

$$x_{n+1} = r x_n (1 - x_n), \qquad r = 1 + a\Delta t. \tag{6}$$

The canonical logistic map is therefore a normalized Euler recurrence. In the untreated derivation above, r is dimensionless and is determined by the intrinsic growth rate and the update interval. It is not, by itself, a dose or efficacy parameter.

4.2 Treatment-dependent formulation

To represent therapy explicitly, it is preferable to formulate the treatment operation first in terms of the dimensional tumor volume T_n. Let g denote the effective untreated growth rate (time^{-1}), Δt_n the interval represented by update n, and $S_n \in (0, 1]$ the surviving fraction associated with treatment during that update. In this manuscript the treatment operation is taken to act after the untreated Euler growth step. The dimensional update is therefore $T_{n+1} = S_n[T_n + g\Delta t_n T_n(1 - T_n/K_c)]$. This ordering is stated explicitly because changing the order of growth and treatment would define a different discrete model.

$$T_{n+1} = S_n \left[T_n + g\Delta t_n T_n(1 - T_n/K_c)\right]. \tag{7}$$

With $y_n = T_n/K_c$, where K_c is fixed, the same update becomes $y_{n+1} = S_n[y_n + g\Delta t_n\, y_n(1 - y_n)]$. This equation is dimensionally consistent for variable Δt_n and does not require a time-dependent normalization. It is the primary treatment-modulated recurrence used for the model formulation. The factor S_n is dimensionless, while $g\Delta t_n$ is dimensionless; consequently the normalized state and the recurrence are dimensionally consistent.

For radiotherapy, the treatment-survival factor can be connected to the linear-quadratic model. For a fraction d_n in Gy, tumor-specific radiosensitivity parameters α and β give the surviving fraction through the linear-quadratic model [10]. If the dose is known and α and β are available, this factor enters S_n directly. The case report provides 26 Gy in five fractions of 5.2 Gy and discusses an α/β ratio of 3.7 Gy for breast tissue. That tissue ratio is not treated here as a tumor-specific radiosensitivity parameter; patient-specific estimation still requires tumor α and β [9].

$$S_{RT,n} = \exp\left[-\left(\alpha d_n + \beta d_n^2\right)\right]. \tag{8}$$

Because the radiotherapy schedule is known but the required tumor-specific radiobiological parameters are not, the radiation equations define a parameterization framework rather than a fitted patient-specific calculation. This distinction also prevents the canonical r values used in the nonlinear benchmark from being interpreted as radiation efficacy estimates.

For chemotherapy, a pharmacodynamic effect may be represented by a saturable exposure-response function [11]. One possible form is the $E_{\max}$ exposure-response relationship, in which C_n is the drug concentration at update n, $E_{\max}$ is a maximum effect rate (time^{-1}), and EC_{50} is the concentration producing half of $E_{\max}$. The coupling between pharmacokinetic exposure and tumor-cell dynamics can be further structured through lifespan-based pharmacokinetic-pharmacodynamic frameworks, in which drug-induced changes in cell turnover are modeled explicitly [12].

$$E(C_n) = \frac{E_{\max} C_n}{EC_{50} + C_n}. \tag{9}$$

A corresponding survival factor over Δt_n is obtained by exponentiating the effective removal or inhibition rate over the interval. Because the survival factor then depends on Δt_n as well as on the pharmacodynamic variables, it must not be treated as an independent uncertainty input when those primitive variables are varied.

$$S_{CT,n} = \exp\left[-E(C_n)\,\Delta t_n\right]. \tag{10}$$

For the present case, the published report does not provide patient-specific plasma concentrations, EC_{50}, $E_{\max}$, or a longitudinal tumor-volume series. Therefore the chemotherapy equations are a parameterization framework, not a fitted patient-specific calculation. The same distinction applies to the radiotherapy parameters.

If chemotherapy and radiotherapy are represented within the same update, their survival factors may be combined multiplicatively when that approximation is justified, giving $S_n = S_{CT,n} S_{RT,n}$. The resulting dimensional and K_c-normalized recurrences remain non-autonomous because the treatment factors and intervals may change from one update to the next.

$$S_n = S_{CT,n} S_{RT,n}, \qquad r_n = (1 + g\Delta t_n)\, S_{CT,n} S_{RT,n}. \tag{11}$$

The expression $r_n = (1 + g\Delta t_n) S_n$ is retained in this work as the control coefficient of a canonical reduced logistic benchmark, not as the exact result of substituting variable Δt_n into the Euler normalization. For a fixed normalization and the canonical reduced

map, $x_{n+1} = r_n x_n(1 - x_n)$. When Δt_n varies in the dimensional model, the exact K_c-normalized equation above should be used. This distinction resolves the normalization ambiguity while preserving a mathematically useful non-autonomous logistic benchmark for the nonlinear analysis.

4.3 Consistent normalization and non-autonomous formulation

With the fixed reference scale K_c, the normalized state $y_n = T_n/K_c$ has a single definition for all updates, even when Δt_n changes. Writing $\kappa_n = g\Delta t_n/(1 + g\Delta t_n)$ and $r_n = (1 + g\Delta t_n)S_n$ gives the equivalent exact form $y_{n+1} = r_n y_n(1 - \kappa_n y_n)$. Thus, the coefficient multiplying the linear term and the coefficient multiplying the quadratic term are both step-dependent. The standard logistic shape $y(1 - y)$ is recovered only in the formal limit $\kappa_n \to 1$, which corresponds to $g\Delta t_n \to \infty$ and is therefore not a physically meaningful continuous limit; for finite Euler steps, the quadratic coefficient κ_n remains strictly less than one. This is why the canonical non-autonomous map is analyzed separately as a reduced mathematical benchmark.

An additional discretization caveat follows directly from the continuous model. The continuous logistic equation has a stable positive equilibrium for $g > 0$, whereas the forward-Euler recurrence can enter period-doubling and chaotic regimes when the dimensionless step is sufficiently large. Those regimes are therefore properties of the discrete approximation at the chosen step size. They should not be interpreted as a prediction that the underlying continuous tumor-growth process, or a patient's tumor, is intrinsically chaotic.

4.4 Non-autonomous state space and extinction criterion

For the canonical non-autonomous benchmark $x_{n+1} = r_n x_n(1 - x_n)$, assume $x_0 \in [0, 1]$ and $0 \le r_n \le 4$ for every n. Since $x_n(1 - x_n) \in [0, 1/4]$, it follows that $0 \le x_{n+1} \le 1$; hence $[0, 1]$ is invariant. If $r_n > 4$ at any update, this invariant-interval argument no longer applies and the normalized biological interpretation requires additional justification.

Near the extinction state $x = 0$, the recurrence satisfies $x_{n+1} = r_n x_n + O(x_n^2)$. More precisely, for $x_n \in [0, 1]$, $x_{n+1} \le r_n x_n$, so $x_N \le x_0 \prod_{n=0}^{N-1} r_n$. For $r_n > 0$, a sufficient condition for asymptotic extinction is

$$\limsup_{N\to\infty} N^{-1} \sum_{n=0}^{N-1} \ln r_n < 0.$$

Under this condition the product decays exponentially and $x_n \to 0$. This is a cumulative condition; requiring $r_n < 1$ at every update is sufficient but is not necessary for non-autonomous extinction. If any $r_n = 0$, extinction occurs immediately from that update onward. Throughout this manuscript, "extinction" refers strictly to the asymptotic mathematical limit $x_n \to 0$ of the canonical normalized recurrence; it does not, by itself, imply complete radiographic, pathological, or clinically meaningful disappearance of a tumor.

For a periodic protocol of period p, with $r_{n+p} = r_n$ and $r_j > 0$, the condition reduces to $(1/p)\sum_{j=0}^{p-1} \ln r_j < 0$, equivalently $\prod_{j=0}^{p-1} r_j < 1$. The product criterion describes local asymptotic stability of the extinction state for the linearized periodic system. If the product is greater than one, extinction is locally unstable. These statements provide a direct mathematical analysis of the treatment-dependent sequence rather than relying only on the autonomous fixed-r map.

As a purely mathematical illustration, the period-two sequences $(0.6, 1.2)$ and $(0.8, 1.5)$ have products 0.72 and 1.20, respectively, in agreement with the logarithmic criterion. The first sequence satisfies the cumulative extinction criterion, whereas the second makes the extinction state locally unstable. These values are illustrative dynamical examples only and are not estimates of the clinical case.

4.5 Fixed points and local stability

The canonical fixed-r analysis is retained as a mathematical benchmark. For constant r, fixed points and their local stability follow from the standard logistic recurrence and provide a reference against which the treatment-dependent formulation can be compared.

For constant r, fixed points satisfy $x^* = rx^*(1 - x^*)$, giving

$$x_1^* = 0, \qquad x_2^* = 1 - \frac{1}{r}. \tag{12}$$

The derivative is $f'(x) = r(1-2x)$. At $x_1^* = 0$, $f'(0) = r$, so the extinction fixed point is locally stable for $|r| < 1$. For the nonzero fixed point, $f'(x_2^*) = 2-r$, which gives stability when $|2 - r| < 1$, i.e. $1 < r < 3$. Therefore the values $r = 2.5$ and $r = 2.8$ do not represent

tumor extinction in the logistic map; they correspond to stable positive equilibria. This point is essential for the biological interpretation and corrects the previous association of decreasing r values with progressively stronger tumor regression.

For a treatment-dependent non-autonomous sequence, the condition $r_n < 1$ at every update is a sufficient pointwise condition for contraction toward extinction in the canonical benchmark, but it is not necessary; the appropriate cumulative criterion is the logarithmic condition given in Sec. 4.4. The canonical values $r = 2.50$–4.00 are therefore not used as proxies for treatment efficacy.

4.6 Parameter definitions and units

Table 2 summarizes the symbols used throughout the manuscript, their units, and their source or interpretation.

5 Clinical Case and Treatment Chronology

The reference clinical case is used as an external treatment chronology rather than as a fully parameterized patient-specific dataset. Hong et al. [9] reported an 83-year-old woman with cT4bN1M1 triple-negative invasive mammary carcinoma and an ulcerated left-breast mass measuring approximately 10×12 cm at presentation. The patient received three cycles of weekly paclitaxel, followed by three cycles of weekly doxorubicin. Because the disease progressed, doxorubicin was stopped and whole-breast radiotherapy was delivered as 26 Gy in five consecutive fractions of 5.2 Gy. Three additional cycles of doxorubicin followed radiotherapy. The systemic therapies and radiotherapy are therefore treated as sequential stages in the clinical chronology, not as simultaneous paclitaxel-plus-radiotherapy updates. Table 3 summarizes the chronology.

The chronology resolves the previous inconsistency: radiotherapy consisted of five fractions, not six. The six values of r used in the nonlinear-dynamics section therefore cannot be labeled as six radiotherapy fractions. They are canonical mathematical parameter values used to sample the known logistic-map regimes. No panel in the revised manuscript is interpreted as evidence of a sixth radiotherapy fraction or of simultaneous paclitaxel and radiotherapy.

6 C++/Geant4 Three-Dimensional Simulation

The C++/Geant4 implementation [13] is retained as a three-dimensional visualization component. The revised mathematical formulation makes an explicit distinction between the scalar global tumor burden and the spatial field needed for voxel-wise coupling. Let $\rho_n(\mathbf{r})$ denote the local normalized tumor-density field in the computational domain Ω. Its global integral is $B_n = \int_\Omega \rho_n(\mathbf{r})\, d\mathbf{r}$; a dimensionless global state can then be obtained by dividing B_n by a fixed reference value. Thus, the scalar x_n and the field $\rho_n(\mathbf{r})$ are different mathematical objects. Geant4 supplies the Monte Carlo radiation-transport environment, but the original exported figures do not contain the voxel-level dose array required for a retrospective patient-specific dose-response calculation. Accordingly, $\rho_n(\mathbf{r})$ is a local voxel-wise field, whereas B_n is a global integral quantity; neither is used interchangeably with the scalar canonical benchmark state x_n.

A fully coupled implementation proceeds locally in space. If $D_n(\mathbf{r})$ denotes the absorbed dose deposited by Geant4 at voxel $\mathbf{r}$ during fraction n, the radiobiological survival factor is

$$S_{RT,n}(\mathbf{r}) = \exp\left[-\alpha D_n(\mathbf{r}) - \beta D_n(\mathbf{r})^2\right]. \tag{13}$$

The local state can then be updated through a K_c-normalized treatment equation, for example $\rho_{n+1}(\mathbf{r}) = S_{RT,n}(\mathbf{r})[\rho_n(\mathbf{r}) + g\Delta t_n \rho_n(\mathbf{r})(1 - \rho_n(\mathbf{r}))]$, subject to the definition and units of the chosen local density variable. If systemic treatment is also represented at that update, its survival factor can be included multiplicatively when the biological approximation is justified.

$$x_{n+1}(\mathbf{r}) = [1 + g\Delta t_n]\, S_{RT,n}(\mathbf{r})\, x_n(\mathbf{r})\, [1 - x_n(\mathbf{r})]. \tag{14}$$

This establishes the mathematical bridge between Monte Carlo dose deposition and local tumor response. A reproducible fully coupled implementation must store the voxel-level dose distribution $D_n(\mathbf{r})$, treatment timing, spatial tumor state, and calibrated biological parameters g, α, and β. The present manuscript does not claim that this coupling was retrospectively applied to the existing Geant4 renderings. Because only rendered outputs, rather than the required voxel dose arrays and synchronized serial imaging, are available in the present dataset, a numerical Geant4 dose-to-response result cannot be reconstructed without introducing unsupported data. We therefore do not fabricate such a calculation;

Table 2. Parameter definitions and units.

Symbol	Meaning	Units	Source/interpretation
$T(t)$	Tumor volume	cm^3 or other volume unit	Measured or reconstructed from imaging
x_n	Normalized state of the canonical logistic benchmark	dimensionless	Scalar state used exclusively in the canonical reduced logistic-map analysis; distinct from the exact K_c-normalized state $y_n = T_n/K_c$
K_c	Continuous carrying capacity	volume	Equilibrium of continuous logistic model
K_E	Euler scaling parameter	volume	Discretization scale; not identical to K_c
a, g	Intrinsic/effective growth rate	$time^{-1}$	Must be estimated from longitudinal tumor data
Δt_n	Interval represented by update n	time	Treatment-cycle/fraction interval
r_n	Treatment-modulated control parameter	dimensionless	Canonical reduced benchmark: $(1 + g\Delta t_n)S_n$; exact K_c-normalized model also depends on κ_n
$S_{RT,n}$	Radiotherapy surviving fraction	dimensionless	LQ model
α	Linear radiosensitivity coefficient	Gy^{-1}	Tumor-specific parameter if available
β	Quadratic radiosensitivity coefficient	Gy^{-2}	Tumor-specific parameter if available
d_n	Radiotherapy dose per fraction	Gy	26 Gy/5 = 5.2 Gy in the case
C_n	Drug concentration	concentration unit	Requires pharmacokinetic data
$E_{\max}$	Maximum chemotherapy effect rate	$time^{-1}$	Requires calibration
EC_{50}	Half-maximal drug-effect concentration	concentration unit	Requires calibration
$\rho_n(\mathbf{r})$	Local normalized tumor-density field	dimensionless	Spatial state used for voxel-wise coupling
B_n	Global tumor burden recovered from the spatial field	volume-equivalent or normalized	$B_n = \int_\Omega \rho_n(\mathbf{r})\, d\mathbf{r}$; a separate fixed reference may define a dimensionless global state
y_n	K_c-normalized tumor volume	dimensionless	Exact normalized state of the treatment-modulated Euler formulation

instead, the coupling is defined explicitly and its validation requirements are stated. The Geant4 component should therefore be interpreted as a mathematical coupling framework for future patient-specific implementation, not as a validated clinical dose–response simulation in the present study.

The three-dimensional figures are therefore presented as clinically inspired computational visualizations. Their density fields are not treated as measured tumor volumes, and the figure labels have been revised to remove the previous implication of simultaneous paclitaxel plus radiotherapy, a sixth radiotherapy fraction, or a quantitative volume-reduction prediction.

Figure 1 presents the initial three-dimensional visualization associated with the radiotherapy stage and establishes the spatial geometry and normalized density-field representation used in the computational workflow. Figure 2 shows an intermediate illustrative state, in which the spatial distribution of the normalized tumor-density field changes within the same computational geometry. Figure 3 presents the final illustrative computational state. The progression across Figures 1–3 is intended to demonstrate the visualization and proposed spatial-response framework only; it is not a reconstruction of measured serial tumor volumes or a patient-specific dose–response trajectory.

7 Nonlinear Dynamics of the Logistic Map

The nonlinear analysis is deliberately separated from the clinical chronology. Its primary role is to validate the numerical implementation against the classical fixed-r logistic map. The bifurcation structure, fixed points, cobweb trajectories, and Lyapunov exponents are established properties of that map and are not claimed as new discoveries. The treatment-dependent non-autonomous sequence $\{r_n\}$, analyzed in Sec. 4.4, is the mathematically relevant extension for changing treatment conditions. Accordingly, Figures 8–7 serve as classical numerical benchmarks and consistency checks; the methodological extension of interest is their separation from, and comparison with, the treatment-modulated non-autonomous framework.

The representative cobweb trajectories in Figures 4–7 provide a geometric view of the dynamical regimes

Table 3. Clinical treatment chronology and its role in the revised model.

Stage	Clinical treatment	Reported schedule	Role in revised model
Initial	Advanced breast tumor	$\sim 10 \times 12$ cm	Initial state/reference geometry
Systemic cycles 1–3	Paclitaxel	Weekly; 3 cycles	Treatment chronology; no patient-specific PK parameters available
Systemic cycles 4–6	Doxorubicin	Weekly; 3 cycles	Treatment chronology; no patient-specific PK parameters available
RT fractions 1–5	Whole-breast radiotherapy	26 Gy in 5×5.2 Gy	Dose input for radiobiological coupling framework
Post-RT	Doxorubicin	3 additional cycles	Later clinical response reference
Follow-up	CT	3.5 months after RT	0.8×1.8 cm reported residual mass

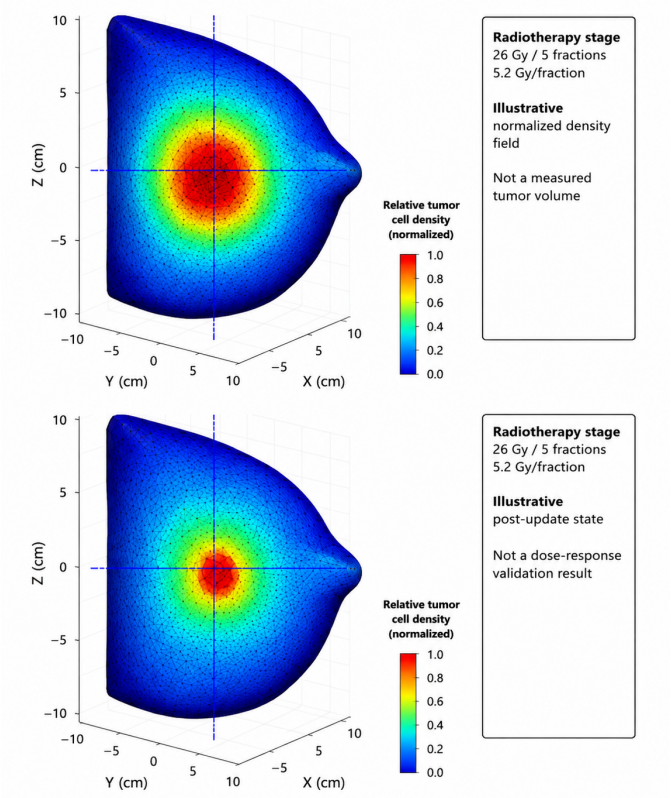

Figure 1. Three-dimensional computational visualization from the radiotherapy stage of the workflow. The systemic therapy preceded radiotherapy in the clinical chronology. The rendering shows a normalized tumor-density field and is not a voxel-level dose-response validation.

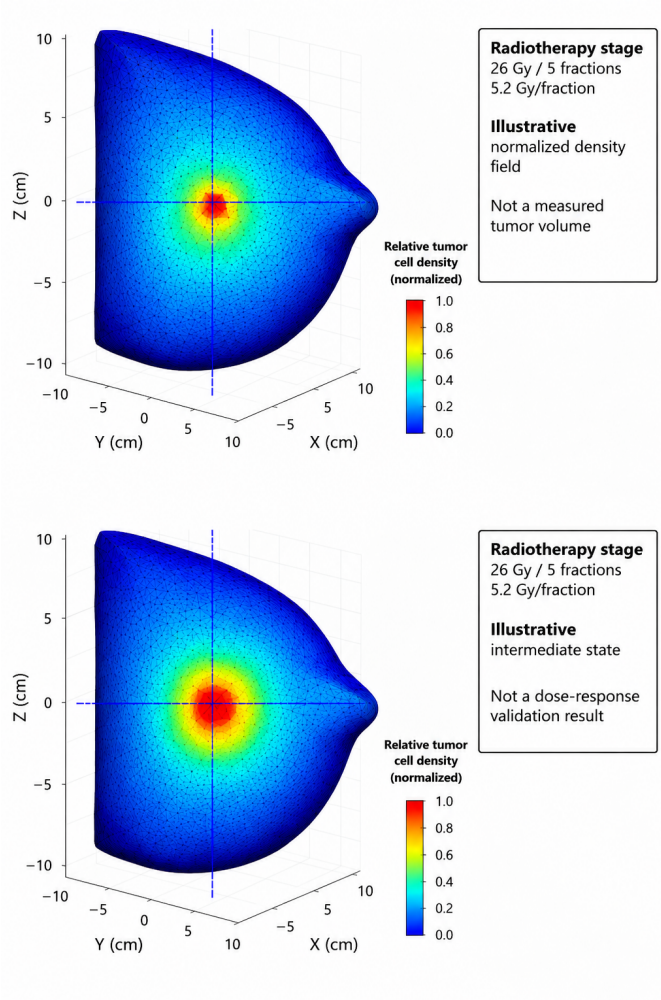

Figure 2. Intermediate three-dimensional visualization from the computational workflow. The panel represents an illustrative normalized tumor-density field during the radiotherapy stage; it is not a measured tumor volume and does not imply simultaneous paclitaxel and radiotherapy.

summarized in Table 4. Figure 4 shows the trajectories for $r = 4.00$ and $r = 3.70$. In both cases, the iterates exhibit nonconvergent behavior associated with the chaotic regimes of the canonical logistic map, consistent with the positive Lyapunov exponents reported in Table 4.

Figure 5 shows the cobweb trajectories for $r = 3.40$ and $r = 3.10$. In contrast to the chaotic cases in Figure 4, the iterates are confined to attracting periodic behavior, consistent with the negative Lyapunov exponents obtained for these parameter values. The

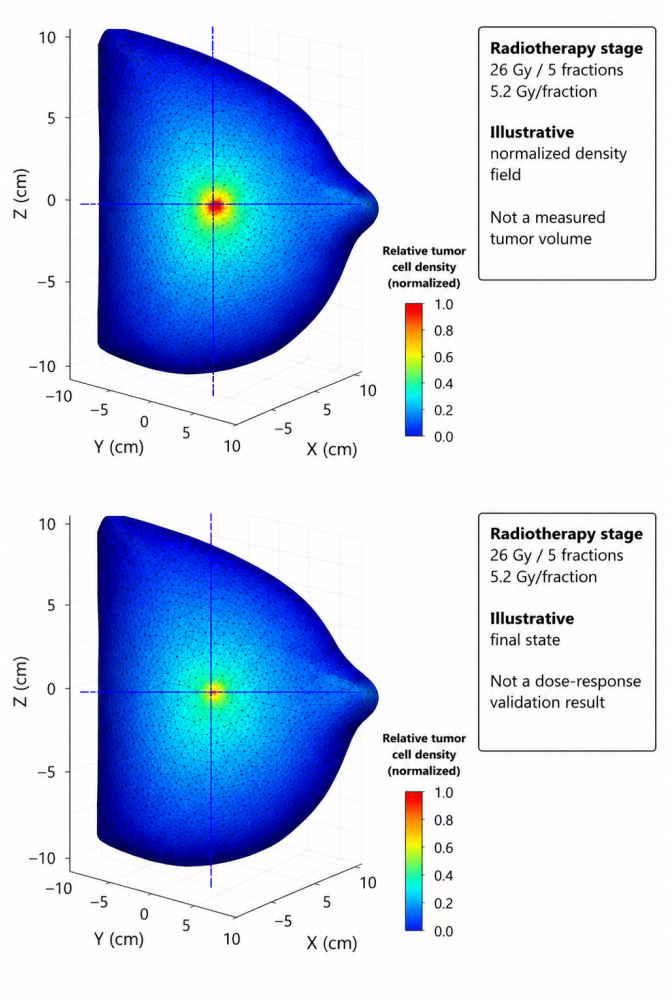

Figure 3. Final three-dimensional visualization from the computational workflow. The right panel is an illustrative final computational state and is not a sixth radiotherapy fraction. The clinical radiotherapy schedule contained five fractions.

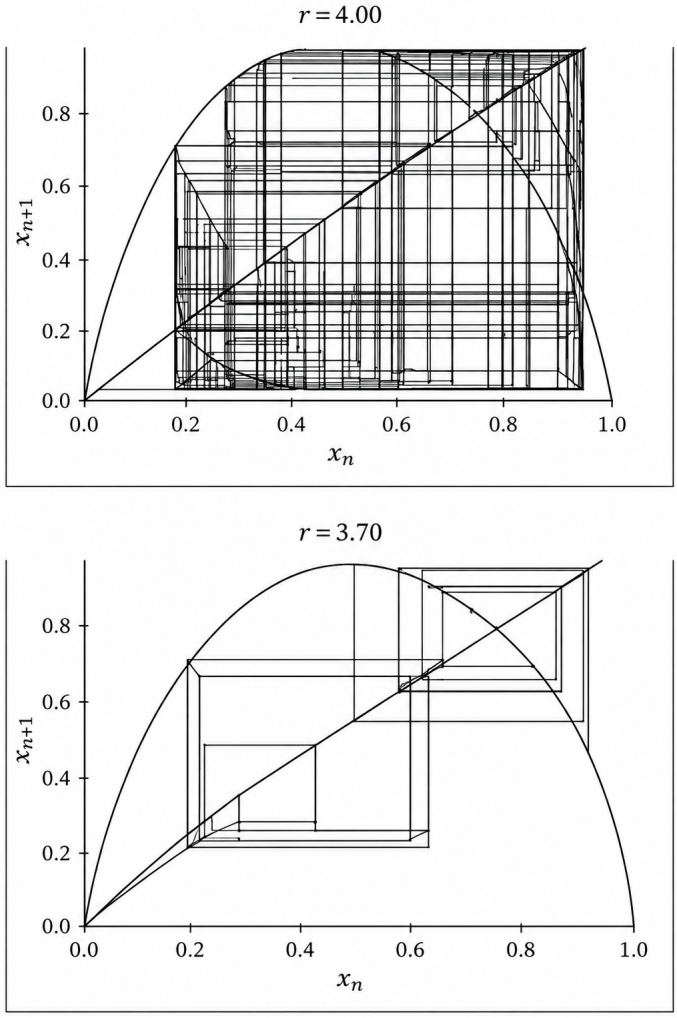

Figure 4. Cobweb trajectories for the canonical logistic regimes $r = 4.00$ and $r = 3.70$. The panels are mathematical demonstrations and are not identified with radiotherapy fractions. These classical trajectories are benchmark calculations used for comparison with the treatment-dependent formulation.

Table 4. Asymptotic regime and Lyapunov exponent for the sampled values of r.

r	**Regime**	λ **(approx.)**	**Interpretation**
4.00	Chaotic	0.6931	Canonical chaotic regime
3.70	Chaotic	0.3513	Canonical chaotic regime
3.40	Periodic	−0.1372	Bounded periodic regime
3.10	Stable period-2 orbit	−0.2638	Stable periodic regime
2.80	Stable fixed point	−0.2231	Stable positive equilibrium
2.50	Stable fixed point	−0.6931	Stable positive equilibrium

comparison between Figures 4 and 5 therefore illustrates the transition from chaotic dynamics to attracting periodic behavior as r is reduced within the canonical benchmark.

At still lower parameter values, the canonical map approaches a stable positive fixed point. Figure 6 shows convergence for $r = 2.80$ toward $x_2^* = 1 - 1/r \approx 0.6429$, whereas Figure 7 shows convergence for $r = 2.50$ toward $x_2^* = 0.6000$. These numerical trajectories are consistent with the analytical fixed-point stability condition $1 < r < 3$ derived in Sec. 4.5. For $r = 2.50$ and $r = 2.80$, the Lyapunov exponents reported in Table 4 also agree with the analytic fixed-point expression $\lambda = \ln|2 - r|$, providing an internal consistency check between Eq. (12), Table 4, and Figures 6–7.

These results are properties of the canonical discrete recurrence and must not be interpreted as evidence of biological chaos or as quantitative treatment-response

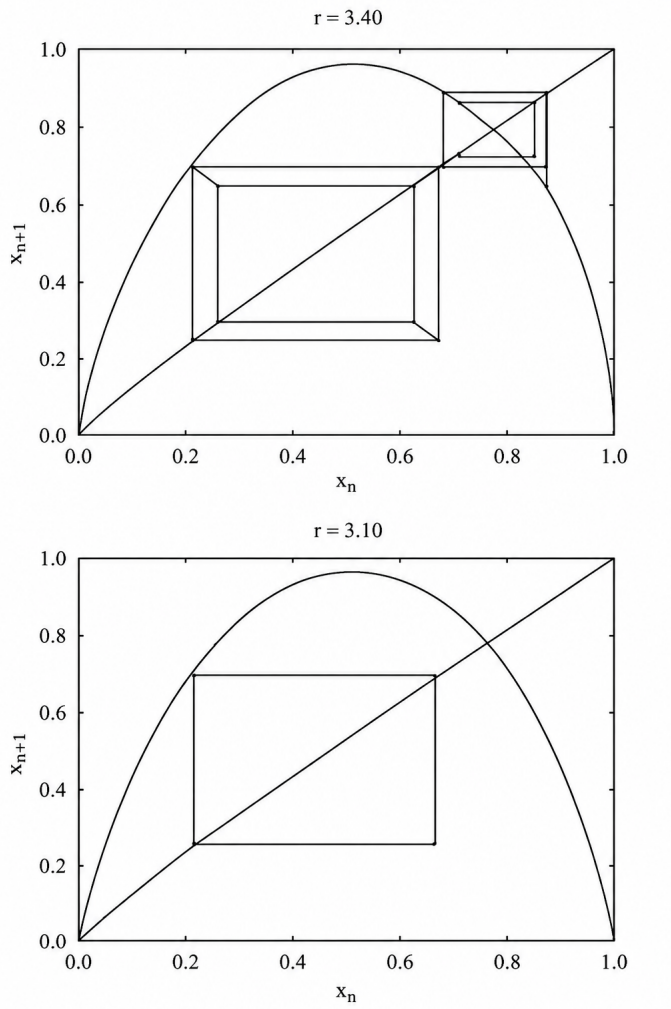

Figure 5. Cobweb trajectories for $r = 3.40$ and $r = 3.10$. The trajectories illustrate periodic and stable behavior of the mathematical recurrence. These classical trajectories are benchmark calculations and are not treatment-response predictions.

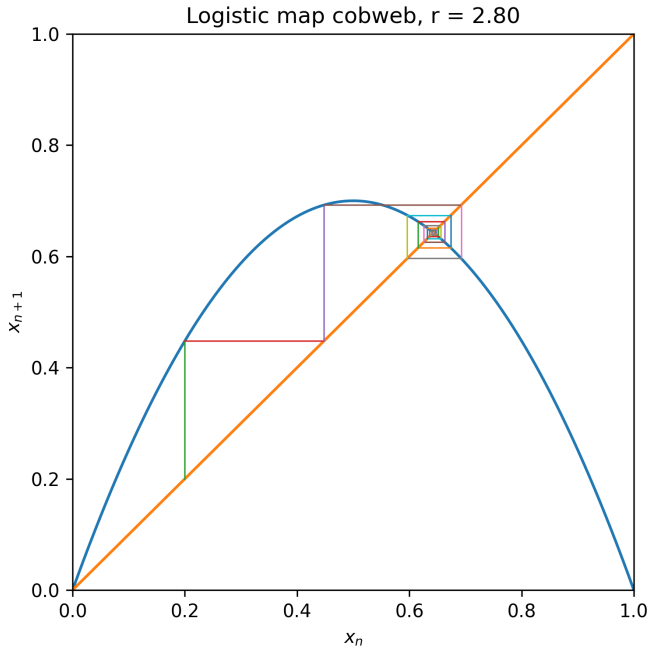

Figure 6. Cobweb trajectory for $r = 2.80$, showing convergence to the positive fixed point $x_2^* = 1 - 1/r \approx 0.6429$. This is a classical benchmark result of the autonomous logistic map and is not interpreted as a clinical endpoint.

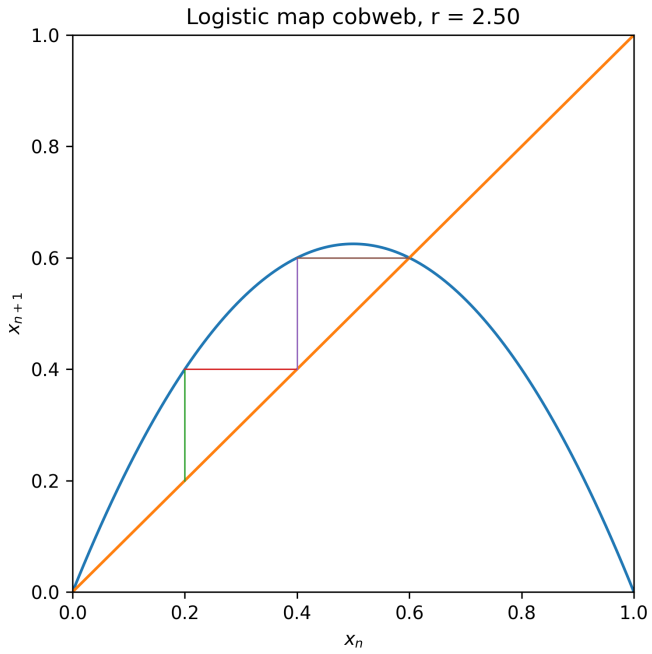

Figure 7. Cobweb trajectory for $r = 2.50$, showing convergence to the positive fixed point $x_2^* = 0.6000$. This is a classical benchmark result of the autonomous logistic map and is not interpreted as a clinical endpoint.

estimates. In particular, the decrease in r across Figures 4–7 represents sampling of different mathematical regimes rather than a sequence of progressively more effective treatment fractions.

The bifurcation diagram in Figure 8 was calculated over the full invariant-interval parameter range $0 \leq r \leq 4.0$ using $x_0 = 0.20$, 2,001 uniformly spaced parameter values, and $\Delta r = 0.002$. The first 1,000 iterations were discarded and 300 subsequent iterates were retained for each r. The diagram recovers the classical transition from fixed-point behavior through successive period-doubling bifurcations to periodic windows and chaotic regimes.

The corresponding Lyapunov-exponent calculation is shown in Figure 9. The exponent was estimated over 10,000 iterations after removal of the first 1,000 transient iterations. Positive values identify parameter regions with sensitive dependence on initial conditions in the canonical discrete map, whereas negative values

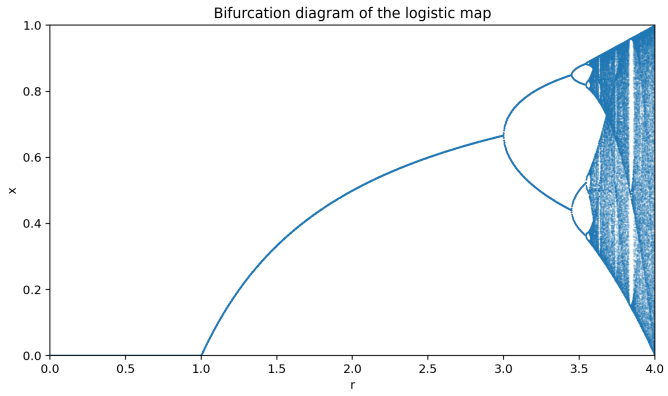

Figure 8. Bifurcation diagram of the canonical logistic map for $0 \leq r \leq 4.0$. For each r, $x_0 = 0.20$; 1,000 transient iterations were discarded, 300 subsequent iterates were retained, and $\Delta r = 0.002$. This classical bifurcation structure is shown as a numerical benchmark and is not claimed as a novel result; its role is to provide a reference for the treatment-dependent non-autonomous formulation.

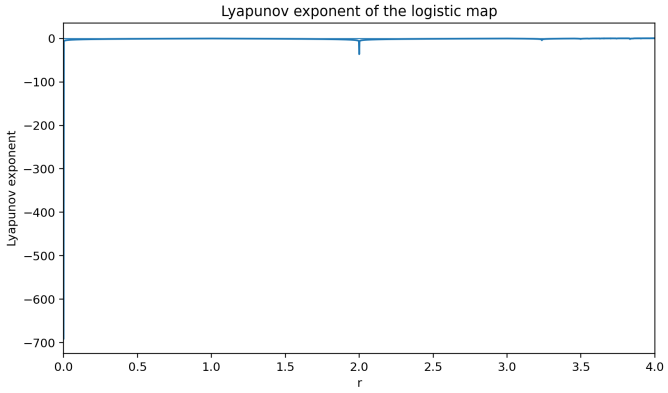

Figure 9. Lyapunov exponent of the canonical logistic map over $0 \leq r \leq 4.0$. Positive values indicate sensitive dependence in the asymptotic discrete dynamics; negative values correspond to attracting periodic or fixed-point behavior. This classical Lyapunov analysis is used as a numerical benchmark for the canonical map and is not itself the novelty of the treatment-modulated framework.

correspond to attracting fixed points or periodic orbits. Figures 8 and 9 are therefore complementary numerical benchmarks: the bifurcation diagram displays the asymptotic states geometrically, while the Lyapunov exponent provides a quantitative indicator of their local dynamical behavior. The full interval is shown because the extinction regime lies below $r = 1$ and because restricting the analysis to $2.5 \leq r \leq 4$ would conceal an important part of the mathematically admissible parameter domain.

7.1 Direct analysis of treatment-dependent sequences

To complement the autonomous benchmark, the canonical non-autonomous recurrence was evaluated with periodic parameter sequences. For a period-two sequence, extinction stability is determined by the product $r_0 r_1$. The illustrative sequences $(0.6, 1.2)$ and $(0.8, 1.5)$ give products 0.72 and 1.20, respectively, in agreement with the logarithmic criterion derived in Sec. 4.4. These computations demonstrate that an individual update may have $r_n > 1$ while the cumulative protocol still satisfies the extinction criterion. Conversely, a sequence with product greater than one makes the extinction state locally unstable. No sequence is fitted to the clinical patient because the required longitudinal data are unavailable.

8 Numerical Algorithm

The fixed-r bifurcation and Lyapunov calculations follow the procedure described in Sec. 3: double-precision arithmetic with $x_0 = 0.20$, 2,001 uniformly spaced values of r on $[0, 4]$ with $\Delta r = 0.002$, 1,000 transient iterations discarded, 300 iterates retained for the bifurcation diagram, and 10,000 iterates used to estimate the Lyapunov exponent by accumulating $\ln |r(1 - 2x_n)|$ after the transient. For the non-autonomous benchmark, r is replaced by the prescribed sequence $\{r_n\}$ and the same recurrence $x_{n+1} = r_n x_n (1 - x_n)$ is iterated in double precision; the illustrative periodic sequences reported in Sec. 7.1 are mathematical tests and are not patient-specific treatment estimates.

9 Clinical Interpretation and Parameter Identifiability

The revised formulation changes the interpretation of r in an essential way. A single constant r cannot simultaneously represent intrinsic tumor proliferation, chemotherapy dose, drug efficacy, radiation dose, radiosensitivity, and treatment interval. Those quantities have different units and enter the biology through different mechanisms. The dimensionless r_n in the canonical benchmark is a composite quantity, while the exact K_c-normalized treatment recurrence also depends on the step-size factor κ_n. Clinical interpretation therefore requires estimation of the primitive biological and treatment variables from longitudinal data.

For chemotherapy, patient-specific estimation requires at minimum a longitudinal tumor-size or cellularity series together with a pharmacokinetic or exposure

surrogate and a specified pharmacodynamic function. Atuegwu et al. [3] demonstrated a clinically grounded strategy in which MRI-derived tumor-cell estimates before and after the first chemotherapy cycle were used to estimate a proliferation rate and predict later cellularity. Their work provides an appropriate precedent for the type of data required to calibrate the present model.

For radiotherapy, the clinical dose schedule is known in the reference case: 26 Gy in five fractions of 5.2 Gy [9]. However, a dose alone does not determine a tumor survival fraction. Tumor-specific α and β are required in Eq. (8). The $\alpha/\beta = 3.7$ Gy value discussed in the case report refers to breast tissue and is therefore not substituted for a tumor-specific value [9].

The reported clinical endpoint is nevertheless useful as an external observed quantity. The case report describes a decrease in the largest reported tumor dimension from approximately 12 cm at presentation to 1.8 cm on CT 3.5 months after radiotherapy. Because the case includes systemic therapy before and after radiotherapy and lacks serial measurements at each treatment update, this endpoint cannot uniquely identify g, chemotherapy survival factors, α, β, or the treatment-dependent sequence. It is not a volume measurement and is therefore not used as an 85% volume-reduction validation target.

This identifiability limitation is not a weakness of the mathematical definition itself; it is a property of the available data. Contemporary analyses of mechanistic tumor models emphasize that parameter identifiability depends on the measurement design and the number and type of time-course observations [6]. The next experimental or clinical stage should therefore collect serial tumor volumes or cellularity measurements synchronized with treatment delivery, together with dosimetric and, when possible, pharmacokinetic information.

10 Discussion

The central mathematical result is the explicit separation between the continuous carrying capacity $K_c = a/b$ and the Euler scaling $K_E = (1 + a\Delta t)/(b\Delta t)$. When the treatment interval varies, K_E also varies, so it cannot serve as a fixed normalization without introducing an additional ratio between successive scales. The revised formulation avoids this ambiguity by normalizing the dimensional treatment update with the fixed continuous carrying capacity K_c.

The second result is the treatment-dependent representation of the canonical reduced coefficient $r_n = (1 + g\Delta t_n)S_n$, together with the exact K_c-normalized recurrence $y_{n+1} = S_n[y_n + g\Delta t_n\, y_n(1 - y_n)]$. This distinction makes clear what is exact and what is a reduced benchmark. It also shows why the fixed sequence $r = 4.00, 3.70, 3.40, 3.10, 2.80, 2.50$ cannot legitimately be interpreted as six progressively more effective treatment fractions.

The third result is the explicit separation of the Geant4 component from the scalar logistic recurrence. Geant4 provides radiation-transport dose deposition, whereas the tumor-response law requires a separate radiobiological mapping from dose to survival and then to the local tumor state. The revised manuscript defines that bridge with a spatial field $\rho_n(\mathbf{r})$, but does not claim a completed patient-specific implementation because the required voxel dose arrays, tumor-specific α and β values, and synchronized serial imaging are not available. Thus, the present Geant4 results constitute a prospective mathematical coupling framework rather than clinical validation of dose–response.

The nonlinear analysis also clarifies the role of chaos theory. The bifurcation diagram and Lyapunov exponent are useful as mathematical verification of the canonical recurrence, but chaotic behavior can arise from the discrete Euler approximation at sufficiently large $g\Delta t$ and should not be interpreted as evidence that a patient's tumor becomes biologically chaotic. The direct mathematical contribution beyond the autonomous benchmark is the treatment-dependent non-autonomous formulation and its cumulative extinction criterion.

Accordingly, the scientific contribution is framed narrowly and defensibly. The work does not claim to have invented the logistic map, discovered its classical bifurcation structure, or produced a patient-specific treatment predictor. Its contribution is a consistent dimensional-to-discrete formulation, an explicit separation between continuous and discretization scales, a direct analysis of treatment-dependent sequences, a dose-to-survival coupling framework for spatial modeling, and a reproducible numerical analysis of the canonical map.

11 Limitations and Requirements for Patient-Specific Validation

- The reference case provides a treatment chronology and selected tumor-size endpoints, but not enough

serial measurements to uniquely estimate all parameters of the treatment-modulated map.

- The case report does not provide the pharmacokinetic concentrations and pharmacodynamic parameters needed to calculate patient-specific chemotherapy survival factors.
- Tumor-specific α and β values are not available in the case report; therefore the radiotherapy survival factor is defined but not fitted to the patient.
- The retained Geant4 figures are clinically inspired three-dimensional visualizations. They are not presented as validated dose-response predictions, and their rendered density values are not treated as quantitatively derived tumor-volume measurements. The local field $\rho_n(\mathbf{r})$ and the global burden $B_n = \int_\Omega \rho_n(\mathbf{r})\, d\mathbf{r}$ are distinct quantities and should not be conflated in interpretation.
- The six canonical r values are mathematical probes of logistic-map dynamics and are not claimed to correspond to the six systemic-therapy cycles or the five radiotherapy fractions.
- Future validation requires synchronized longitudinal imaging, voxel-level treatment dose maps, independent estimation or measurement of biological parameters, and uncertainty/sensitivity analysis propagated from the primitive inputs rather than from dependent composite quantities.

11.1 Quantitative clinical consistency and uncertainty analysis

The available clinical case permits only an observed dimensional consistency check, not a patient-specific validation of the treatment-modulated recurrence. The reported largest tumor dimension decreased from approximately 12 cm at presentation to 1.8 cm on CT 3.5 months after radiotherapy. The ratio $1.8/12 = 0.15$ corresponds to a relative reduction of $1 - 1.8/12 = 0.85$, or approximately 85%, in the largest reported dimension. This is a one-dimensional clinical endpoint; it is not a reconstructed tumor volume. Because the treatment sequence is multimodal and serial measurements are unavailable, the endpoint is not used to fit r_n or to claim model validation. Therefore, all references to the 12 cm-to-1.8 cm change in this manuscript denote change in the largest reported tumor dimension, never a change in tumor volume.

The uncertainty analysis is formulated in terms of primitive inputs [14]. For chemotherapy, take $\theta_{CT} = (g, \Delta t_n, C_n, E_{\max}, EC_{50})$, with $E(C) = E_{\max} C/(EC_{50} + C)$, $S_{CT,n} = \exp[-E(C_n)\Delta t_n]$, and $r_n = (1 + g\Delta t_n) S_{CT,n}$ for the canonical reduced benchmark. The relevant derivatives are $\partial r_n/\partial g = \Delta t_n S_{CT,n}$; $\partial r_n/\partial \Delta t_n = S_{CT,n}[g - (1+g\Delta t_n)E(C_n)]$; $\partial r_n/\partial E_{\max} = -(1 + g\Delta t_n) S_{CT,n} \Delta t_n C_n/(EC_{50} + C_n)$; $\partial r_n/\partial C_n = -(1 + g\Delta t_n) S_{CT,n} \Delta t_n E_{\max} EC_{50}/(EC_{50} + C_n)^2$; and $\partial r_n/\partial EC_{50} = (1 + g\Delta t_n) S_{CT,n} \Delta t_n E_{\max} C_n/(EC_{50} + C_n)^2$. These derivatives avoid treating $S_{CT,n}$ as independent of its primitive inputs.

$$\sigma_{r_n}^2 \approx (\Delta t_n S_{CT,n})^2 \sigma_g^2 + (g S_{CT,n})^2 \sigma_{\Delta t_n}^2 + (1 + g\Delta t_n)^2 \sigma_{S_{CT,n}}^2. \tag{15}$$

For radiotherapy, use $\theta_{RT} = (g, \Delta t_n, \alpha, \beta, d_n)$, $S_{RT,n} = \exp[-\alpha d_n - \beta d_n^2]$, and $r_n = (1 + g\Delta t_n) S_{RT,n}$ in the canonical reduced benchmark. The corresponding derivatives are $\partial r_n/\partial g = \Delta t_n S_{RT,n}$; $\partial r_n/\partial \Delta t_n = g S_{RT,n}$; $\partial r_n/\partial \alpha = -d_n(1 + g\Delta t_n) S_{RT,n}$; $\partial r_n/\partial \beta = -d_n^2(1 + g\Delta t_n) S_{RT,n}$; and $\partial r_n/\partial d_n = -(\alpha + 2\beta d_n)(1 + g\Delta t_n) S_{RT,n}$. A first-order covariance propagation can then be written as $\mathrm{Var}(r_n) \approx J_n \Sigma_\theta J_n^T$, where J_n is the gradient with respect to the primitive parameter vector and Σ_θ is its covariance matrix. If correlations are unknown, they must not be silently assumed absent; an independence assumption is an additional modeling choice that must be stated. In both treatment cases, θ denotes the primitive-parameter vector, $J_n = \partial r_n/\partial \theta$ is the corresponding row Jacobian (gradient), and Σ_θ denotes the covariance matrix of that same primitive vector; this notation is used consistently throughout the uncertainty analysis.

The clinical endpoint is therefore retained only as an observed external quantity, while numerical uncertainty intervals are reserved for a future patient-specific dataset containing the required inputs.

The state-level sensitivity is propagated recursively for the canonical non-autonomous map. For any primitive parameter θ, define $s_n = \partial x_n/\partial \theta$. Then $s_{n+1} = x_n(1 - x_n)\, \partial r_n/\partial \theta + r_n(1 - 2x_n) s_n$, with $s_0 = \partial x_0/\partial \theta$. This recursion quantifies how uncertainty in primitive treatment and biological inputs accumulates through the nonlinear state dynamics. For the exact K_c-normalized recurrence, the analogous sensitivity is obtained by differentiating $y_{n+1} = S_n[y_n + g\Delta t_n\, y_n(1 - y_n)]$ with respect to the same primitive vector.

When serial tumor-volume measurements become available, model accuracy can be quantified by the normalized root-mean-square error

$$\mathrm{NRMSE} = \frac{\mathrm{RMSE}}{T_{\max} - T_{\min}}, \tag{16}$$

where $T_{\max}$ and $T_{\min}$ denote the maximum and minimum observed tumor volumes in the longitudinal series, and RMSE is the root-mean-square deviation between model predictions and measurements. This metric is reserved for future patient-specific validation once the required serial data are available; it is not applied to the present dataset, for which only a single endpoint measurement is reported.

12 Conclusion

The logistic map remains a useful discrete nonlinear system for studying cycle-based tumor dynamics, but its biological interpretation requires an explicit and dimensionally consistent parameterization. The revised formulation distinguishes the continuous carrying capacity K_c from the Euler scaling K_E and, when treatment intervals vary, avoids using a time-dependent Euler scale as though it were a fixed normalization.

Treatment is first formulated in dimensional tumor volume and then normalized by K_c, yielding the exact update $y_{n+1} = S_n[y_n + g\Delta t_n\, y_n(1-y_n)]$. The canonical coefficient $r_n = (1+g\Delta t_n)S_n$ is retained as a reduced non-autonomous logistic benchmark. The manuscript derives invariant-state and cumulative extinction conditions for $\{r_n\}$, including the periodic product criterion, and explicitly distinguishes sufficient pointwise conditions from necessary cumulative conditions. Here, "extinction" is a mathematical asymptotic property of the normalized recurrence and is not equated with clinical disappearance of disease.

Chemotherapy and radiotherapy enter through treatment-specific survival factors, while the Geant4 component is connected to a spatial tumor-density field through a dose-to-survival relation. The available clinical case does not provide enough data for patient-specific calibration or retrospective voxel-level validation, so the manuscript does not fabricate such results. The reported 12 cm to 1.8 cm change is correctly described as an 85% reduction in the largest reported tumor dimension, not in tumor volume. The canonical bifurcation and Lyapunov calculations are presented as mathematical verification, with the main contribution centered on the consistent treatment-dependent formulation and its direct non-autonomous analysis. The Geant4 coupling is therefore presented as a framework for future patient-specific implementation rather than as a validated clinical dose–response simulation.

Data Availability Statement

Data will be made available on request.

Funding

This work was supported without any funding.

Conflicts of Interest

The author declares no conflicts of interest.

AI Use Statement

The author declares that generative artificial intelligence (ChatGPT) was used for language editing and consistency checking of the manuscript. The authors have carefully reviewed, revised, and verified the AI-assisted output and take full responsibility for the content of the manuscript.

Ethical Approval and Consent to Participate

Not applicable. This study involved only a secondary theoretical analysis of a previously published, de-identified clinical case report and did not involve the recruitment or experimentation of new human participants or animals.

References

[1] Siegel, R. L., Kratzer, T. B., Giaquinto, A. N., Sung, H., & Jemal, A. (2025). Cancer statistics, 2025. *CA: A Cancer Journal for Clinicians, 75*(1), 10. [CrossRef]

[2] Kim, J., Harper, A., McCormack, V., Sung, H., Houssami, N., Morgan, E., ... & Fidler-Benaoudia, M. M. (2025). Global patterns and trends in breast cancer incidence and mortality across 185 countries. *Nature medicine, 31*(4), 1154-1162. [CrossRef]

[3] Atuegwu, N. C., Arlinghaus, L. R., Li, X., Chakravarthy, A. B., Abramson, V. G., Sanders, M. E., & Yankeelov, T. E. (2013). Parameterizing the logistic model of tumor growth by DW-MRI and DCE-MRI data to predict treatment response and changes in breast cancer cellularity during neoadjuvant chemotherapy. *Translational oncology, 6*(3), 256-264. [CrossRef]

[4] Pearl, R., & Reed, L. J. (1920). On the rate of growth of the population of the United States since 1790 and its mathematical representation. *Proceedings of the national academy of sciences, 6*(6), 275-288. [CrossRef]

[5] May, R. M. (1976). Simple mathematical models with very complicated dynamics. *Nature, 261*(5560), 459-467. [CrossRef]

[6] González Vázquez, A., & Villaverde, A. F. (2025). Analysing the structural identifiability and observability of mechanistic models of tumour growth. *Bioengineering*, *12*(10), 1048. [CrossRef]

[7] Jiménez, R. P., & Hernandez, E. O. (2011). Tumour–host dynamics under radiotherapy. *Chaos, solitons & fractals*, *44*(9), 685-692. [CrossRef]

[8] Zahid, M. U., Mohsin, N., Mohamed, A. S., Caudell, J. J., Harrison, L. B., Fuller, C. D., ... & Enderling, H. (2021). Forecasting individual patient response to radiation therapy in head and neck cancer with a dynamic carrying capacity model. *International Journal of Radiation Oncology* Biology* Physics*, *111*(3), 693-704. [CrossRef]

[9] Hong, Y., Nixon, N., Cao, J. Q., & Lee, S. L. (2023). Case report: ultrahypofractionated palliative breast radiotherapy for a fungating invasive mammary carcinoma. *Frontiers in Oncology*, *13*, 1171444. [CrossRef]

[10] Fowler, J. F. (1989). The linear-quadratic formula and progress in fractionated radiotherapy. *The British Journal of Radiology*, *62*(740), 679-694. [CrossRef]

[11] Mould, D. R., Walz, A. C., Lave, T., Gibbs, J. P., & Frame, B. (2015). Developing exposure/response models for anticancer drug treatment: special considerations. *CPT: pharmacometrics & systems pharmacology*, *4*(1), 12-27. [CrossRef]

[12] Mo, G., Gibbons, F., Schroeder, P., & Krzyzanski, W. (2014). Lifespan based pharmacokinetic-pharmacodynamic model of tumor growth inhibition by anticancer therapeutics. *PLoS One*, *9*(10), e109747. [CrossRef]

[13] Agostinelli, S., Allison, J., Amako, K., Apostolakis, J., Araujo, H., Arce, P., … & Zschiesche, D. (2003). Geant4—a simulation toolkit. *Nuclear Instruments and Methods in Physics Research Section A: Accelerators, Spectrometers, Detectors and Associated Equipment*, *506*(3), 250–303. [CrossRef]

[14] Burgos-Simón, C., Cortés, J. C., Martínez-Rodríguez, D., & Villanueva, R. J. (2020). Modeling breast tumor growth by a randomized logistic model: A computational approach to treat uncertainties via probability densities. *The European Physical Journal Plus*, *135*(10), 826. [CrossRef]

Matheus dos Santos Farias Holds a Bachelor's degree and a teaching qualification in Physics from the Institute of Physics at the University of São Paulo (IF-USP). Conducted research in Applied Physics—specifically within groups focusing on differential equations applied to health, hadron therapy, and cardio-vascular biomechanics and is a member of the American Physical Society (APS). A specialist in Medical Physics (certified by Albert Einstein Israelite Hospital - HIAE), he has conducted research in proton therapy, delay differential equations, and dynamical systems (chaos theory). His clinical experience covers diagnostic radiology including quality control, image quality optimization, and performance assessment for X-ray, CT, mammography, fluoroscopy, and MRI systems as well as nuclear medicine (involving radiopharmaceuticals, internal dosimetry, and equipment quality control) and radiotherapy (radiotherapy planning, linear accelerator calibration, brachytherapy, and dose distribution verification). He also has experience in radiation protection applied to medical physics and is a member of the American Association of Physicists in Medicine (AAPM). Currently pursuing a Master's degree in Nuclear Physics at the Institute for Energy and Nuclear Research (IPEN-USP), he conducts research with an emphasis on delay differential equations and dynamical systems (chaos theory). He worked on developing an equation to predict the size of gold nanoparticles (AuNPs) for nanobrachytherapy applications in biomedicine, in international scientific collaboration with University College London (UK). He is a member of the American Nuclear Society (ANS) and the SIAM Activity Group on Dynamical Systems. Laboratory experience in the synthesis of gold (AuNPs), silver (AgNPs), and copper (CuNPs) nanoparticles, as well as their physicochemical characterization using UV-Vis spectroscopy, Dynamic Light Scattering (DLS), Transmission Electron Microscopy (TEM), Scanning Electron Microscopy (SEM), X-Ray Diffraction (XRD), Zeta Potential, and Fourier-Transform Infrared Spectroscopy (FT-IR); expertise in mathematical modeling (analytical and numerical simulation), data analysis, and programming using LaTeX, Python, R, C, C++, MATLAB, Wolfram Mathematica, and Monte Carlo methods (PENELOPE, TOPAS, MCNP); and application of Machine Learning and AI techniques in nuclear, biomedical, and medical fields.